The following chapter contains material adapted in part, with permission, from:

Journal of Physical Chemistry C, 114 (28) 12300–12307, Jun 28 2010

http://pubs.acs.org/articlesonrequest/AOR-2zUgS72Z5YFJiekWnC5S

Chapter 3

Electrical Measurements I: Surface Conductance

3.1 Introduction

The electrical defects that are associated with either physical defects or chemical impurities at the surface can have a profound impact upon the electrical characteristics of a semiconductor material. These defects may form electrical states within the bandgap that can capture or emit electronic carriers, which can cause deviations from expected behavior of electrical contacts, as well as provide a relaxation pathway for free carriers. This section outlines the origin of the parameters used to quantify the electronic properties of the the Ge(111) surface as a function of the chemical surface conditions.

3.1.1 Surface Recombination

3.1.1.1 Background

Even for an electrically isolated semiconductor, there must be an eventual relaxation to equilibrium after a perturbation, such as a light pulse in the case considered here. Relaxation through non-radiative, trap-assisted recombination was first modeled by Shockley and Read, and independently by Hall, and is commonly referred to Shockley-Read-Hall (SRH) recombination. The rate of relaxation depends upon the concentration of conduction band electrons (n), valence band holes (h), recombination-generation (R-G) centers, both empty and filled (p_T and n_T, respectively), and proportionality constants describing the rate of electron capture and emission ($c_n$and e_n) and hole capture and emission ($c_p$and e_p). This net recombination is expressed as[1,2]

$$\begin{aligned} r_n &= \frac{\delta n}{\delta t}|_{R-G} = c_n p_T n - e_n n_T \\ r_p &= \frac{\delta p}{\delta t}|_{R-G} = c_p n_T p - e_p p_T \end{aligned} \tag{3.1}$$

Equation 3.1 is generally applicable to any situation involving a non-degenerate semiconductor. If the simplifying assumption is made that the capture and emission coefficients remain constant under both equilibrium ($r_n = r_p = 0$) and non-equilibrium conditions, the emission terms may be rewritten as capture terms dependent upon the R-G center position within the bandgap.

$$e_n = c_n \left(\frac{p_T n}{n_T} \right) = c_n n_1 \tag{3.2a}$$

$$e_p = c_p \left(\frac{n_T p}{p_T} \right) = c_p p_1 \tag{3.2b}$$

where through the relations

$$n_1 \equiv \frac{p_T n}{n_T}$$

$$p_1 \equiv \frac{n_T p}{p_T}$$

$$N_T \equiv n_T + p_T$$

$$n_1 = \left(\frac{N_T}{n_T} - 1 \right) n = \left[\left(1 + \exp \frac{(E_T - E_F)}{kT} \right) - 1 \right] n_i \exp \left[(E_F - E_i) / kT \right]$$

$$n_1 = n_i \exp \left[(E_T - E_i) / kT \right] \tag{3.2c}$$

$$p_1 = n_i \exp \left[(E_i - E_T) / kT \right] \tag{3.2d}$$

Equations 3.1 and 3.2 concern the crystal bulk, but analogous relations can be drawn for surface processes, though the trap and carrier concentrations are in terms of area rather than volume.

$$r_{ns} = c_{ns}\left(p_{Ts}n_s - n_{Ts}n_{1s}\right) \tag{3.3a}$$

$$r_{ps} = c_{ps}\left(n_{Ts}p_s - p_{Ts}p_{1s}\right) \tag{3.3b}$$

For steady-state conditions, $r_{ns} = r_{ps}$ and a general recombination rate can be defined, after rearranging equation 3.3a to replace n_{Ts} & p_{Ts} with N_{Ts}, as

$$R_s = \frac{n_s p_s - n_i^2}{\frac{1}{c_{ps}N_{Ts}}\left(n_s + n_{1s}\right) + \frac{1}{c_{ns}N_{Ts}}\left(p_s + p_{1s}\right)} \tag{3.4}$$

where the factors $(cN_T)^{-1}$have units of velocity, and in the absence of complicating factors such as high-level injection or surface fields, represent the flow of carriers to the surface. Equation 3.4 is valid for the case of a single trap-state level, however real surfaces have a continuum of states so that N_{Ts} is correlated to a density of states, $D_T(E)dE$, integrated over the entire bandgap and R_s becomes

$$R_s = \int_{E_V}^{E_C} \frac{n_s p_s - n_i^2}{\frac{1}{c_{ps}}(n_s + n_{1s}) + \frac{1}{c_{ns}}(p_s + p_{1s})} D_T(E)dE \tag{3.5}$$

For low-level injection ($\Delta n_s = \Delta p_s \ll n_{s0}$), the steady-state carrier concentrations can be related to the equilibrium concentrations through

$$n_s = n_{s0} + \Delta p_s \tag{3.6a}$$

$$p_s = p_{s0} + \Delta p_s \tag{3.6b}$$

$$n_s p_s - n_i^2 = n_{s0} \Delta p_s \tag{3.6c}$$

and $R_s$can be rewritten in terms of the perturbation Δp_s

$$R_s = \left[\int_{E_v}^{E_C} (c_{ps} D_T) \left(1 + \frac{n_{1s}}{n_{s0}} + \frac{c_{ps} p_{1s}}{c_{ns} n_{s0}} \right)^{-1} dE \right] \Delta p_s = s_p \Delta p_s \tag{3.7}$$

The bracketed integral in equation 3.7 depends only upon the surface state distribution, so it is taken as a system parameter, s_p, known as the surface recombination velocity (for n-type samples in this case).

3.1.1.2 Photoconductivity Decay

Recombination center density can be measured, by way of the surface recombination velocity, through photoconductivity decay (PCD) profiles. Excess carriers generated by a rapid light pulse raise the conductivity of the semiconductor. After the pulse, the conductivity will decrease to the original value at a rate defined by the rate of recombination both in the bulk and at the surface. Single-crystal Si and Ge can be prepared with sufficiently high quality that bulk recombination is low and surface recombination dominates. The effective carrier lifetime τ is obtained from the decay constant seen in the PCD profile of conductance as a function of time

$$y(t) = Ae^{-\frac{t}{\tau}} + C \tag{3.8}$$

Because carriers require a finite amount of time to diffuse to the surface, τ is dependent upon the sample geometry. For the case of a wafer with an area that is wide compared to the distance a carrier may traverse, but a thickness that is not, that dependence may be eliminated by converting τ to the surface recombination through

$$\frac{1}{\tau} = \frac{1}{\tau_{bulk}} + \frac{2s}{d} \tag{3.9}$$

where d is the sample thickness, and the factor 2 is due to the sample having two surfaces.

The derivation of s leading to equation 3.7 assumed restrictive conditions of low-level injection and flat bands, but is often extended to arbitrary conditions.[1] For the SiO_x/Si interface, the band-bending is not severe and the capture cross-sections of the electrons and holes are similar for the dominant recombination center, so the surface trap density, N_{Ts}, can be fairly approximated by the relation

$$s = \sigma \upsilon_{th} N_{Ts} \tag{3.10}$$

where σ is the carrier capture cross-section and υ_{th} is the thermal drift velocity.

3.1.2 Surface Charging

Surface states with slow kinetics for one carrier type are not efficient recombination centers, but still interfere with electrical contact formation. While the barrier height of the junction should depend upon the work function of the contacting phase, surface states that accept or donate the charge that would have ideally resided throughout the space-charge region. The resulting insensitivity of the junction properties to the contacting phase is known as *Fermi level pinning.* Fermi level pinning is a well-known feature of metal/Si Schottky diodes. The pinning is believed to arise from formation of silicides during the metal deposition process.[2] Room temperature, solution-phase contacts could be formed without reactive conditions of high temperatures at the silicon surface. More recently, soft contact formation has been explored so that the degree of pinning is not so dependent on contact formation conditions.[3–5]

3.1.2.1 Surface Conductance

The experiment described in this section is designed to measure the charged surface states and associated surface potential. Sample conductance is measured as the surface potential is varied by means of a field plate parallel to the sample surface.[6]

The surface charge associated with the trap states results in carrier concentrations near the surface that are different than those in the bulk. This can be measured as a change in conductance, σ, according to[7]

$$\Delta\sigma = q\left(\mu_n \Delta N + \mu_p \Delta P\right) \tag{3.11}$$

where ΔN and ΔP are the total change in electron and hole concentrations within the near-surface region.

$$\Delta N = \int_0^\infty (n - n_b) dz \tag{3.12a}$$

$$\Delta P = \int_0^\infty (p - p_b) dz \tag{3.12b}$$

The factors μ_n and μ_p are surface mobilities, less than or equal to the bulk mobilities, the exact values depend upon the nature of the surface scattering. The deviation from bulk values is greatest in strong inversion or accumulation. Under circumstances closer to flat-band conditions, equation 3.11 is a direct measure of surface potential reflected in the carrier concentrations.

Figure 3.1 on page 67 is a plot of $\Delta\sigma$ as a function of surface potential v_s for a lightly doped n-type sample at room temperature. At flat-band conditions, the excess surface carrier density is zero, so this is taken as the reference point. For positive surface potentials, accumulation conditions exist and the excess electrons raise the total measured surface conductance. Similarly, for sufficiently negative surface potentials, inversion conditions exist and the excess hole concentration is high enough to raise the sample conductance. At less negative potentials, the surface region is depleted of majority carriers, and there is an insufficient concentration of minority carriers to compensate, so the sample conductance is decreased.

For a sample of uniform composition and thickness, the conductance may be

related to the measured resistance by

$$\Delta\sigma = \frac{l^2}{A}\left(\frac{1}{R} - \frac{1}{R_0}\right) \tag{3.13}$$

where l is the sample length, $A = l \times w$ is the area of the sample faces. It is difficult to predict $R_o$within the necessary accuracy, but if the semiconductor dopant density is known, the potential at which the surface crosses from depletion to inversion can be calculated, and the point of maximum *resistance* can be used to connect the measured resistance values with the calculated relationship in Figure 3.1 on page 67 by rearranging equation 3.13 to

$$\Delta\sigma - \Delta\sigma_{min} = \frac{l}{2w}\left(\frac{1}{R} - \frac{1}{R_{max}}\right) \tag{3.14}$$

3.1.2.2 Pulsed Fields

If the surface field is varied over a timescale that is fast compared to the recombination processes associated with the surface-states, more information can be gained before steady-state conditions are re-established. If a surface under inversion can be made to rapidly enter accumulation by means of an external field, the excess surface charges responsible for the inversion conditions will be emitted into the near-surface region of the bulk, where they contribute to the carrier concentration, resulting in an initial rise in conductance. The conductance will reach steady-state conditions with a decay constant dependent upon recombination processes, very similar to what is seen for the light pulse response in the PCD measurements. Unlike the PCD, where

the magnitude of the response (parameter A) of equation 3.8) is dependent upon the intensity of the light pulse, the magnitude of the pulsed field response is dependent upon the concentration of excess charge in the inversion layer.

In the case of an n-type sample, inversion conditions would arise from the presence of negatively charged acceptor states, and the positive minority carriers associated with the inversion layer that counters the surface states. At the onset of a positive pulse to the surface, the positive charge of the inversion layer is injected into the bulk. Negative charges enter through the ohmic contacts to counter the injected charge. Negative charges also flow to the surface region to counter the positive field plate, but these are accounted for in the steady-state conductance that is eventually reached. The difference between the peak conductance just after the field pulse and the final steady-state conductance is therefore

$$\delta\sigma = q(\mu_n + \mu_p)\Delta P \tag{3.15}$$

where ΔP is the excess positive charge of the inversion layer, and the mobilities have their usual bulk values.

3.2 Experimental

PCD and surface conductance measurements were performed simultaneously with a setup (depicted in Figure 3.3 on page 71) based off of the experiments of Montgomery and Brown.[6] Each sample was an approximately 22 × 12 mm piece of double-side polished wafer. Prior to any chemical treatments, a 1–2 mm region was sanded at

Figure 3.1: Surface conductance vs surface potential

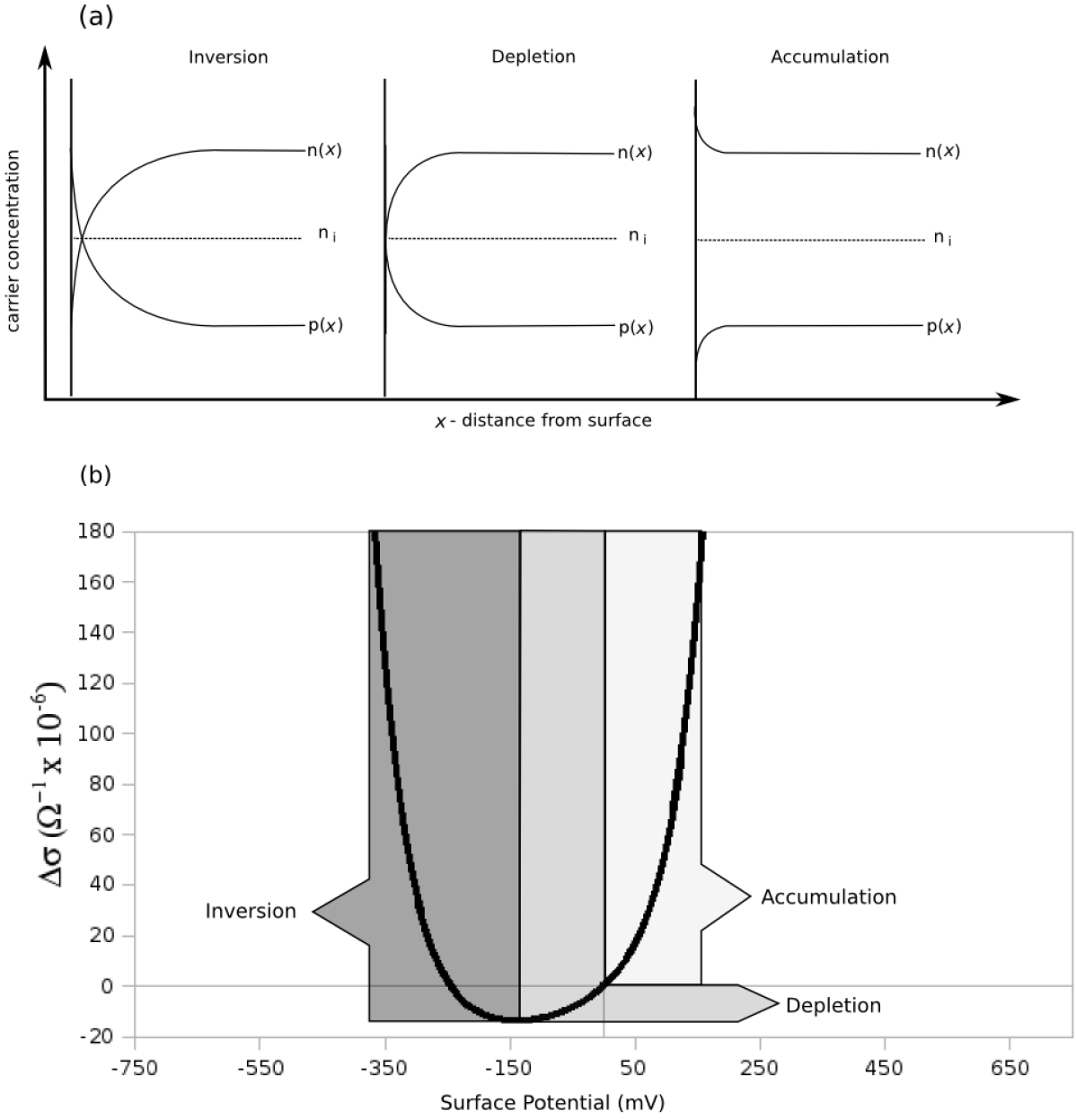

the two shorter edges in order to facilitate ohmic contact formation. After the chemical treatments described in Chapter 2, the ohmic contacts were formed by applying either Ga/In eutectic or Pb/Sn solder.

A gate region was formed on each side of the substrate by clamping the sample between two transparent conductive oxide-coated glass plates. The plates were separated from the Ge surface by a 10–13 micron thick polyvinyl fluoride film (Goodfellow) coated with hydrocarbon oil to exclude air from gaps. The resulting capacitance was approximately 400 pF/cm^2. One end ohmic contact was grounded while the other was connected to a constant-current source. The voltage drop across the sample between the ohmic contacts was continuously monitored with a TDS210 oscilloscope (Tektronix). The gate voltage was supplied by two 2.5 W $\pm$1kV power supplies (Matsusada JB-1N, JB-1P), and controlled by a custom built circuit. The magnitude of the bias was manually adjusted from 0 - $\pm$800 V. The gate bias waveform consisted of 50% duty cycle, 10–20 ms period square wave with pulses of alternating sign.

Photogeneration of carriers for PCD was achieved with a 20–30 ns pulse of 1550 nm light from a laser diode (Laser Components, Inc.), powered by an Electro-Optic Devices ETX-10A laser driver, directed through one of the field plates. The pulse was fired 1–3 ms after the onset of the gate bias. Low-level injection was confirmed from the peak conductance value, which indicated a photogenerated carrier density of $\leq 10^{12}$cm^{-3}.

For each measured gate voltage, the waveform was signal averaged and stored digitally. The photogenerated transient present in the waveforms were fit to equation 3.8. The voltage at the field-free region was set to zero, and the offset parameter

C was used to determine the change in surface conductance. For each sample, each surface conductance value was recorded, with its corresponding SRV, into a two-column .csv file and converted to surface potential using the Python script in the Appendix. Figure 3.2 is a plot of the correlation calculated with the script and used for the conversion.

3.3 Results

All samples modified through the two-step halogenation which displayed no evidence of oxidation in the XP spectra were found to have a p-type surface (inversion conditions), in agreement with the original ethylation.[8] Surfaces that did display some oxidation were in depletion or accumulation. Hydrogen- and bromine-terminated surfaces were not stable for the conditions or time-scale of the experiment, so they were not measured. Samples that did display oxidation in the XP spectra, including methanethiol-terminated and hydrogermylated samples, showed n-type surfaces (accumulation conditions).

3.3.1 Surface Conductance

Figure 3.12 on page 84 is a plot of the measured surface recombination as a function of surface potential. Samples that displayed very low recombination velocities had no clear maximum. Oxidized samples show low recombination values, but the surface charging is too severe to measure flat-band conditions, so meaningful measurements were not possible. The plotted surface potential values for the oxidized sample were

Figure 3.2: Conductance curves for the Ge (a) and Si (b) substrates used. The solid line is the more heavily doped of the pair.

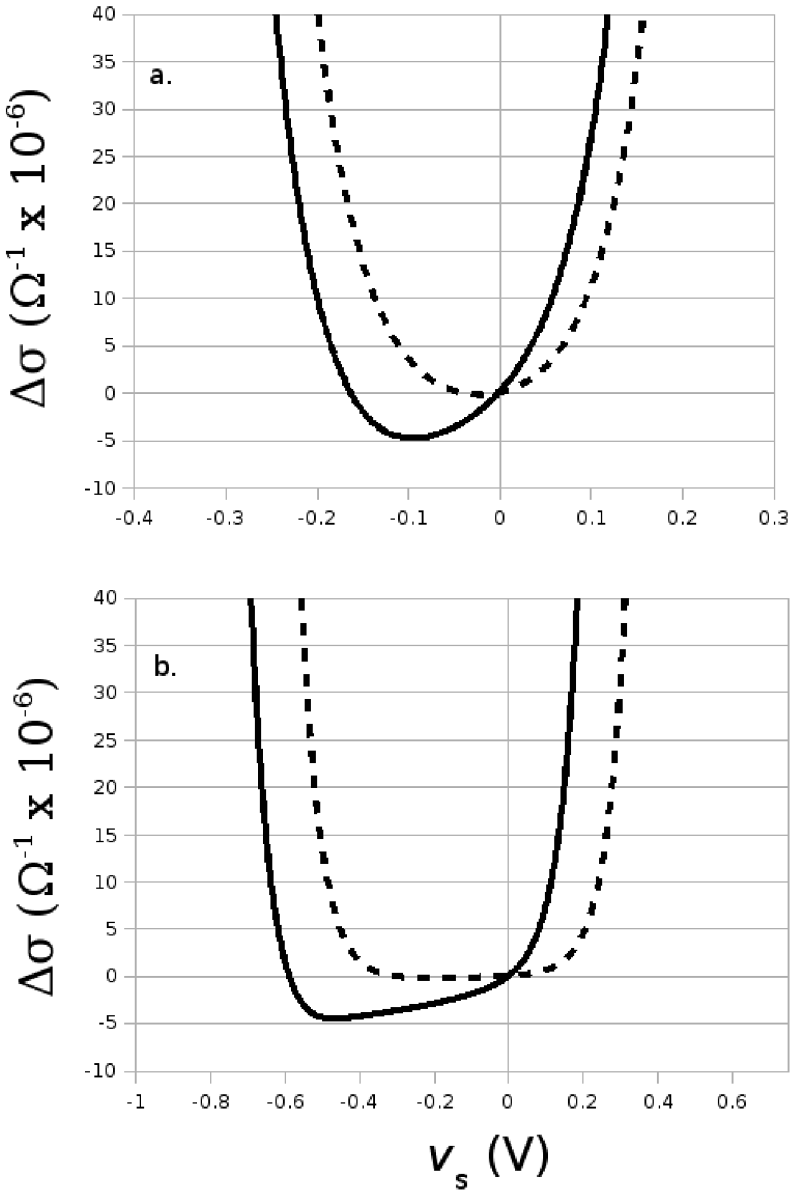

Figure 3.3: Experimental setup

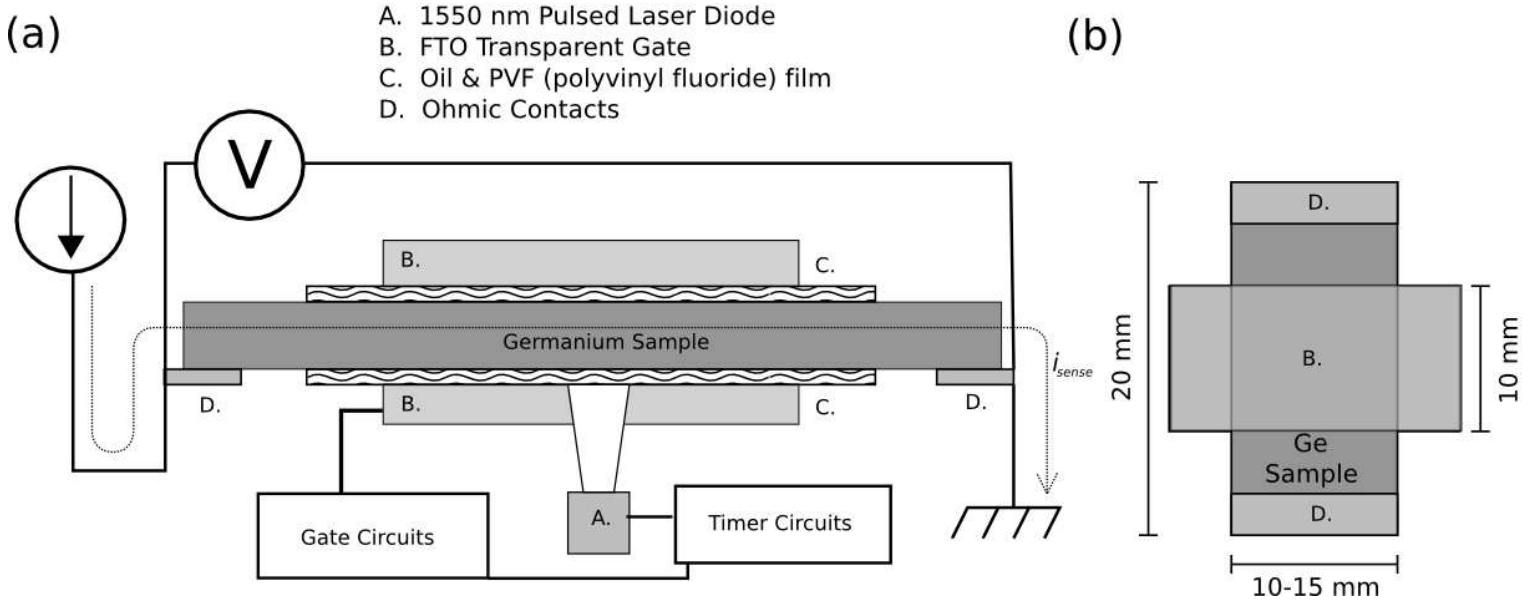

not quantitatively accurate, but serve to illustrate that the oxidized surfaces were under accumulation conditions.

Surface potentials at no applied field and the maximum SRV values of all samples for which the point of minimum conductance and maximum recombination could be reached are collected in Table 3.1. The general trend is that methyl-terminated samples had higher surface charging than the ethyl- and decyl-terminated surfaces, but the surface recombination is lower, even as the surface is brought to flat-band conditions.

3.3.2 Pulsed Fields

Lightly doped n-type methyl- and ethyl-terminated surfaces were under inversion, so the surface charge density could be extracted directly from the transient response to the application of a positive gate bias. Figures 3.4 and 3.5 show the recorded waveforms of the conductance of a methyl-terminated surface in response to a positive and negative gate bias, respectively. The onset of the positive bias in Figure 3.4 coincides with peak 1. The change in conductance from the height of peak 1, to the baseline that follows is dependent upon the excess charge in the inversion layer as given by equation 3.15. Peak 2 is the conductance transient from the optical injection of the laser pulse. The excess charge density was found to be as high as 10^{12} charges per square centimeter for methyl-terminated samples.

The conductance responses of oxidized Ge(111) to a positive and negative gate bias are shown in Figures 3.6 and 3.7, respectively. These waveforms display a dif-

ferent sign in the response to the bias, indicating the surface is not under inversion conditions.

3.3.3 Silicon

CH_3-Si(111) showed similar results to those seen on Ge(111), but it was not possible to span the much larger bandgap by means of the field plate and the point of minimum resistance could not be reached. The experimental configuration was also not well-suited to the high resistance of lightly doped Si, which caused the RC time-constant of the conductance circuit to be of similar magnitude to the time-scales of interest. Qualitative information could still be gained from the sign of the surface conductance response to a gate bias. High resistivity n-type CH_3-Si(111) showed conductance modulations very similar to what is seen in Figures 3.4 through 3.7. Figure 3.8 displays the response of such a surface to a negative gate bias. Due to the RC time-constant, the capacitive spikes at the beginning and end of each gate bias pulse had a noticeably longer duration, but were still useful to confirm that the surface conductance response was of the same sign as that observed in Figure 3.7. Figure 3.9 shows the response of of an native oxide Si(111) surface, from the same wafer, to the same gate bias. The response is opposite that of the methyl-terminated surface and of the same sign as the oxidized Ge(111) surfaces. Moderately doped 70 Ohm-cm n-type Si did not show inversion waveforms. Figures 3.10 and 3.11 show the conductance responses to a negative gate bias of a CH_3-Si(111) and a SiO_x-Si(111), respectively. The capacitive spikes are much narrower because of the lower resistivity of the Si

samples. The conductance waveforms do not follow the square wave bias because of relaxation due to surface states associated with carrier recombination or generation, which are in greater number on the oxidized surface and therefore produce a faster relaxation. Despite the relaxation, the signs of the responses can still be seen to be opposite the responses of the higher resistivity Si(111) From Figure 3.2, this would indicate the surface potential of the high-resistivity CH_3-Si(111) is more negative than -200 mV, and that the surface potential of the moderately doped CH_3-Si(111) surface is less negative than -400 mV.

Figure 3.4: Conductance waveform of CH_3-Ge(111) surface in response to positive gate bias

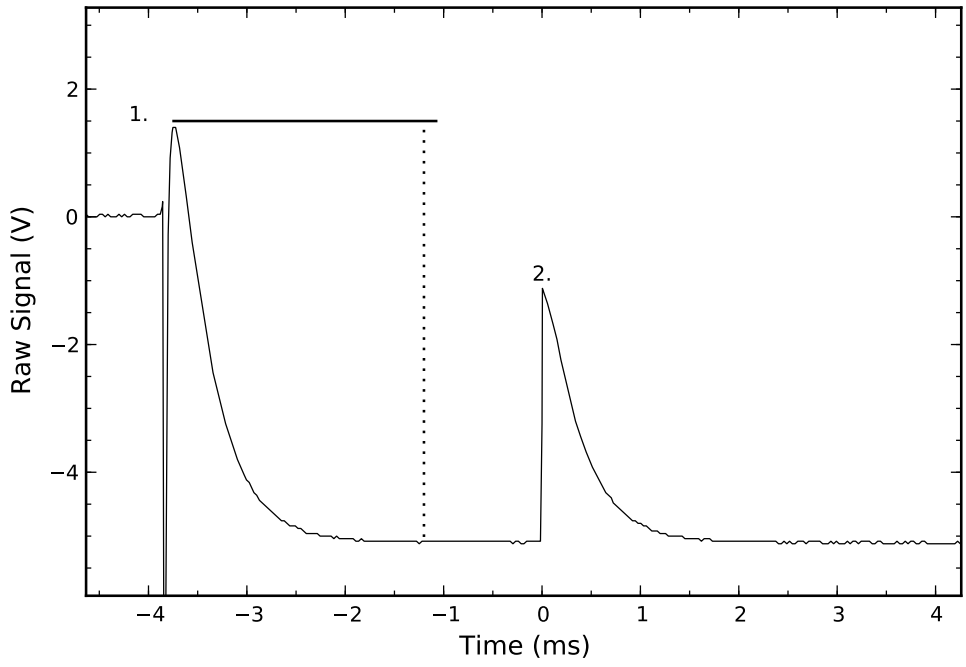

Figure 3.5: Conductance waveform of CH_3-Ge(111) surface in response to negative gate bias

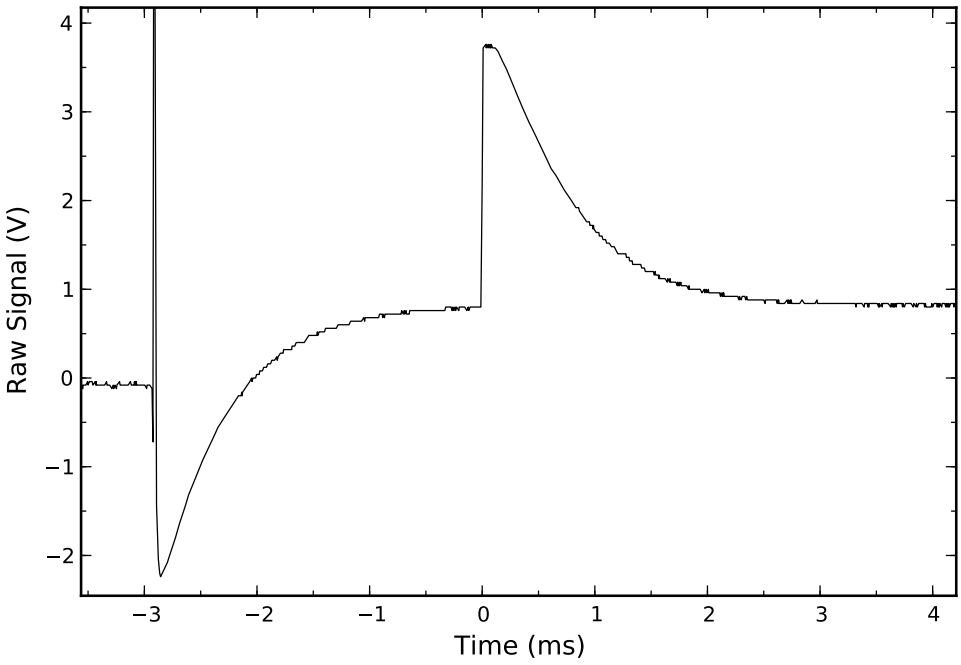

Figure 3.6: Conductance waveform of GeO_x-Ge(111) surface in response to positive gate bias

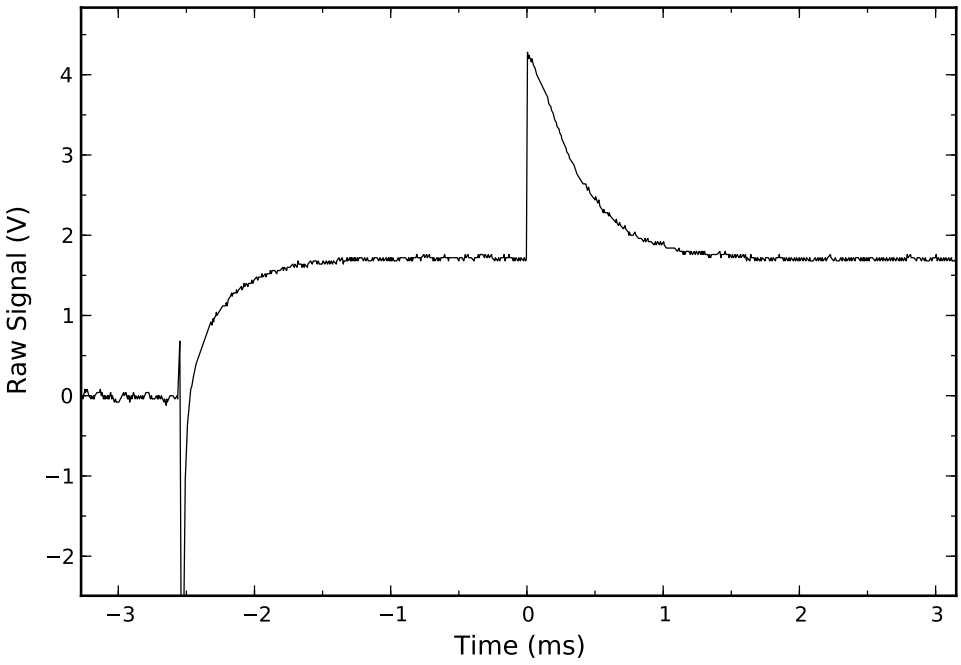

Figure 3.7: Conductance waveform of GeO_x-Ge(111) surface in response to negative gate bias

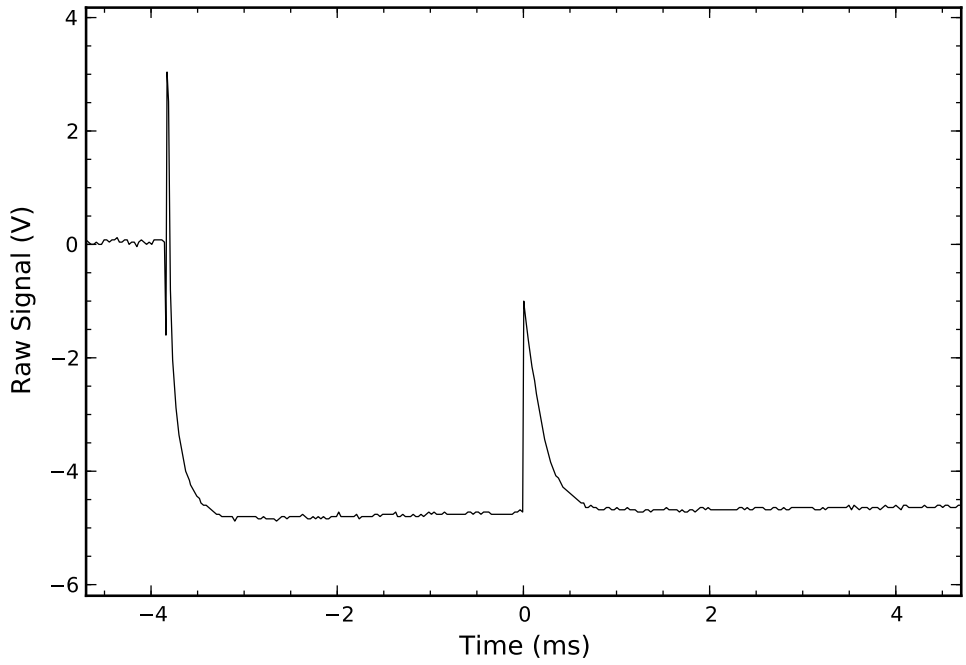

Figure 3.8: Negative gate bias applied to CH_3-Si(111) (N_D=4×10^{11}cm^{-3})

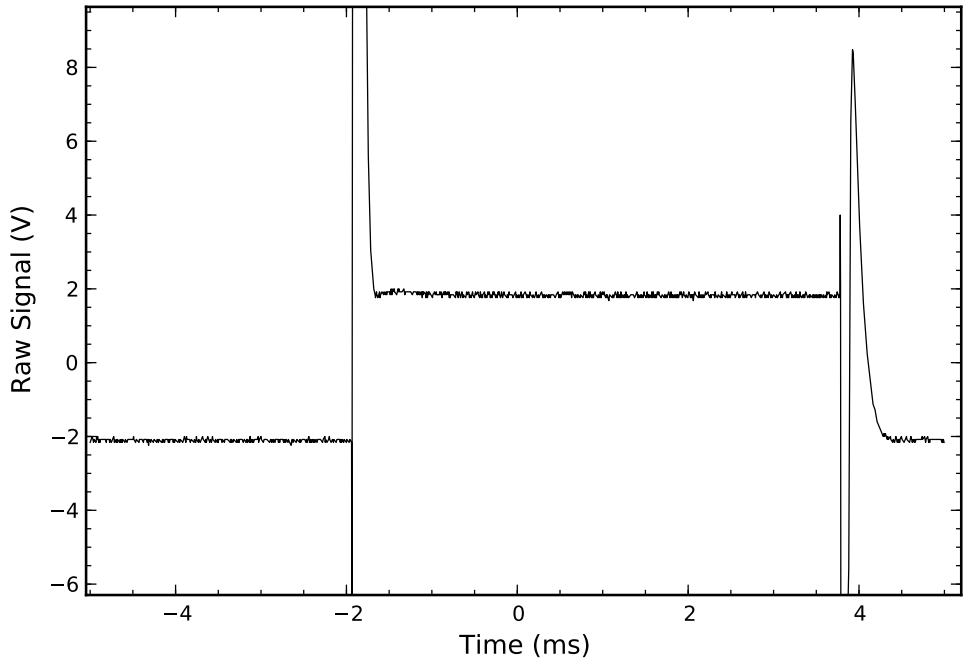

Figure 3.9: Negative gate bias applied to SiO_x-Si(111) (N_D=4×10^{11}cm^{-3})

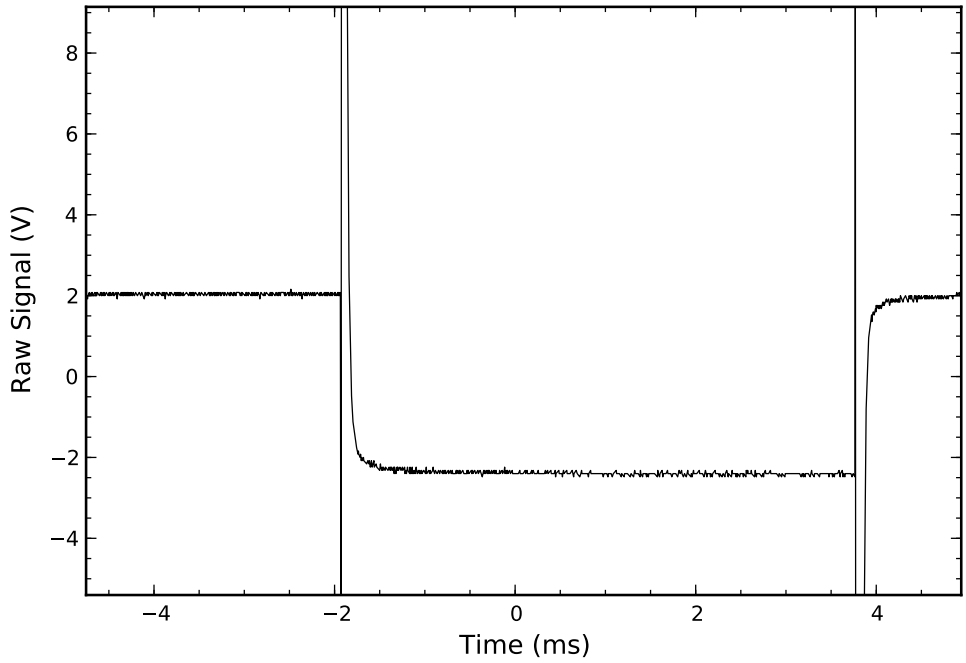

Figure 3.10: Negative gate bias applied to CH_3-Si(111) (N_D=7×10^{13}cm^{-3})

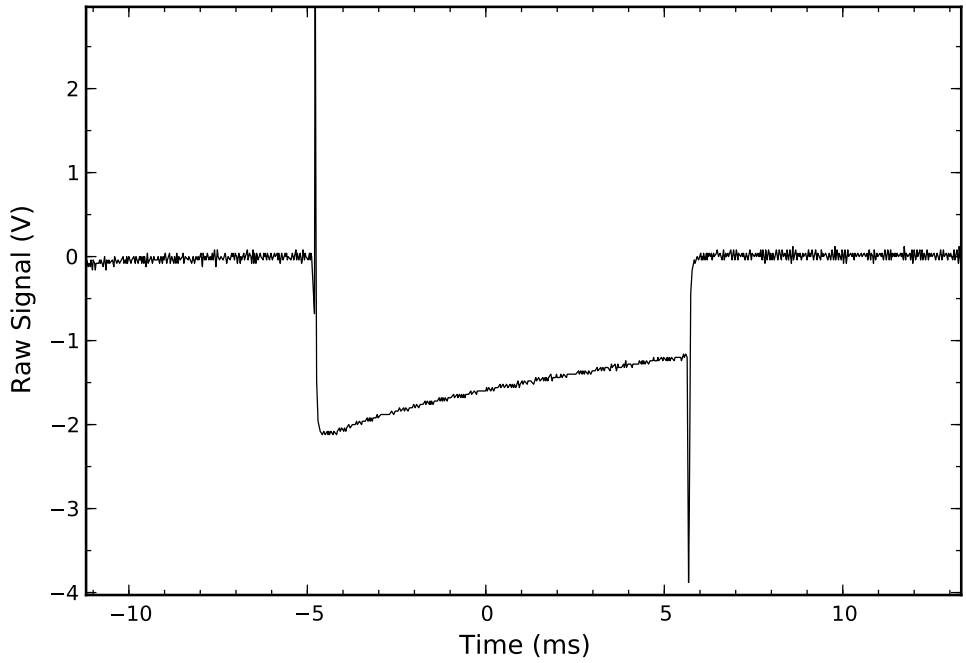

Figure 3.11: Negative gate bias applied to SiO_x-Si(111) (N_D=7×10^{13}cm^{-3})

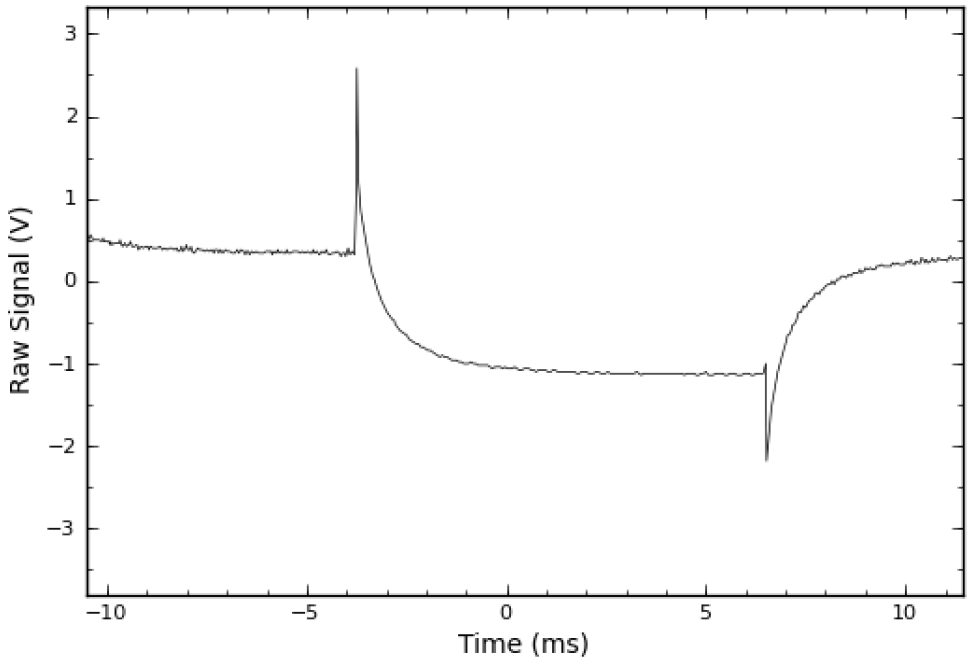

3.4 Discussion

The very low surface recombination measured for methyl- and ethyl-terminated surfaces indicate the halogenation/alkylation method is effective in passivating R-G centers at the surface. The oxidized samples displayed low recombination, but no conclusions can be drawn concerning R-G centers. While the photovoltage generated in high-level injection conditions would have countered the surface potential, the resulting PCD constant would have been a function of both electron and hole lifetimes.[9] If the majority carriers, in this case the electrons, have slower recombination kinetics (a low c_{ns} of equation 3.5) the effective lifetime will be dominated by the slower majority carrier recombination as the surface states are saturated.[10] To keep the measured recombination a function of the sample and not injection level, low-level injection conditions were maintained.

The opposing trends in surface charging and SRV seen in the alkylated surfaces suggest that slight oxidation could be responsible for the less severe band-bending in decyl- and ethyl-terminated surfaces. While relatively recent photoelectron measurements of valence band shifts in oxidizing Ge tend not to support the notion that the oxide is responsible for the positive shift in surface potential for n-type material, it should be noted that such measurements must be performed under UHV conditions.[11–14] It has long been known that water vapor makes an oxidized Ge surface more n-type, and the surface conductance measurements were performed in standard laboratory atmosphere.[6,15] While the sign of the surface potential is consistent with the original ethylation, it is not what would be expected if the methyl groups were

Table 3.1: Equilibrium Surface Potential and Maximum SRV

Sample #	D-1-0	E-1-1	E-1-2	E-1-3	M-1-4	E-2-1	E-2-2	M-2-3
$v_{s,0}$(mV)	-140	-50	-140	-220	-270	-100	-100	-270
SRV_{max} (cm/s)	520	450	210	224	50	230	350	170
Sample #	E-2-4	M-2-5	E-2-6	M-3-1	E-3-2	M-3-3	E-3-4	M-3-5
$v_{s,0}$(mV)	-100	-250	-210	-210	-140	-260	-170	-260
SRV_{max} (cm/s)	480	100	300	140	130	70	150	70

Figure 3.12: Surface recombination vs surface potential

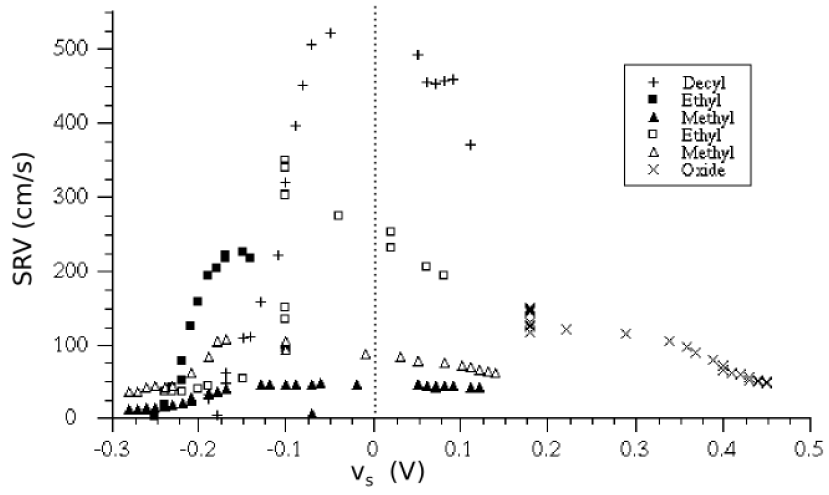

eliminating dangling bonds, based upon theoretical calculations and experimental observations of Ge field effect transistors.[16,17] If the conclusion is that, for methyl-terminated surfaces, the oxide has been eliminated but there still exist dangling bond defects with a density of 10^{12}cm^{-2}, this would imply a deficit in the passivating monolayer on the order of 1%. Such a density is below the detection limit of the available XPS data for these particular surfaces.

A comparison to methyl-terminated silicon is useful because CH_3-Si(111) is a well-studied surface.[18–20] The effective surface passivation by methylation seen in Si(111) has been attributed to the elimination of dangling bonds. Because the molecular geometry for CH_3-Si(111) and CH_3-Ge(111) are so similar, it would be thought that methylation would have a similar effect on dangling bonds of a Ge surface. Conductance experiments performed on CH_3-Si(111) suffered some experimental draw-backs. Intrinsic Si is much more resistive than intrinsic Ge, so time resolution was lost because of the resulting high RC element of the detection circuit. More highly doped material requires stronger fields to span the range of accumulation to inversion conditions. The fields used in this experiment, which were not adequate, were already greater than 200 kV/cm, far exceeding the dielectric strength of the soft hydrocarbon and fluorocarbon spacers necessary to avoid shorting to and damaging the surface. Within the limitations, however, the sign of the conductance response to pulsed fields could still be used to determine which arm of the conductance curve (see Figure 3.2 on page 70) the surface was at. Because the high resistivity material showed inversion conditions, the surface potential had to be more negative than -200 mV. The more highly doped n-type silicon did not show inversion conditions, so the surface potential

had to be less negative than -460 mV. This is not in disagreement with photoelectron measurements indicating a negative surface potential of as much as 200 mV.[18,21]

Reports of inversion layers in the chlorinated Si(111) surface raise the question of whether small amounts of halogen atoms are unreacted and causing the negative surface potential.[22] The authors ascribe the observed increase in conductance of Cl-Si(111) relative to H-Si(111) to an inversion layer caused by electron-withdrawing chlorine produced positive holes in the n-type Si. The increased conductance could be caused by an inversion layer, but it could also be caused by an accumulation layer or a surface film. Aside from measuring the decrease in conductance as the chlorine layer degrades in air, the authors did not modify the surface potential, but subsequent UHV STS measurements showed no clear bandgap, which indicated a density of states within the bandgap, which could give rise to an inversion or accumulation layer.[23] The amount of charge in the inversion layer present in the methyl-terminated surface is consistent with 0.1–1% of the Ge(111) surface atoms remaining halogen-terminated. Such a concentration is well below the detection level of the XPS, but is not insignificant. However, the lack of observation of persistent chlorine atoms in similarly prepared methyl-terminated Si(111) samples, for which there is also a shift in surface potential, makes it unlikely that unreacted halogen surface atoms are the cause of the surface charge.[18,20,21,24]

An increase in work function of 1.2-1.5 V was observed for the Cl-Si(111) surface by Lopinski et al., but work function-dependent measurement techniques would be sensitive to the surface dipole, and the authors did not make the distinction.[18,22,25,26] The surface conductance measurements performed here should not be sensitive to sur-

face dipoles because the current used to measure the surface conditions flows parallel to the surface, rather than crossing the interface. Surface fields are applied across the interface, but the magnitude of the bias voltage is never used directly in calculating the surface potential. The band positions would be affected if the semiconductor was in thermal equilibrium with the field-plate conductor, however the 20 micron thick insulator makes the semiconductor insensitive to the conductor work function.

3.5 Conclusion

Alkylated surfaces prepared through the two-step halogenation/alkylation display surface electronics that are quite distinct from the oxidized starting material. Methyl-terminated Ge(111) surfaces show very little surface recombination, but have a surface potential approaching -300 mV. Bulkier alkyl groups are comparable, but show slightly higher SRV and lower surface potential. Oxidized surfaces and all other surfaces, including hydrogermylated surfaces, showed a positive surface potential, but the surface charging was too severe to determine a definite value. The negative surface potential of the methyl-terminated surface is consistent with elimination of states associated with a hydrated oxide, but could be indicative of surface-states located near the valence band.

Silicon surfaces show a similar degree of band-bending, consistent with earlier photoelectron measurements. This is significant because it means that the two-step alkylation is successful for Ge(111) as it is for Si(111), despite the less atomically smooth surface and the unstable H-Ge(111) precursor surface.

Bibliography

[1] Pierret, R. *Advanced Semiconductor Fundamentals*; Addison-Wesley Publishing Co.: Reading, Mass., 1989; Vol. 6.

[2] Sze, S. *Physics of Semiconductor Devices*, 2nd ed.; John Wiley & Sons: New York, 1981.

[3] Maldonado, S.; Plass, K.; Knapp, D.; Lewis, N. *J. Phys. Chem. C* **2007**, *111*, 17690–17699.

[4] Choi, J.; Ahmed, S.; Dimitrova, T.; Chen, J.; Schroder, D. *IEEE Trans. Electron Dev.* **2004**, *51*, 1380–1384.

[5] Sharp, I.; Schoell, S.; Hoeb, M.; Brandt, M.; Stutzmann, M. *Appl. Phys. Lett.* **2008**, *92*, 223306.

[6] Montgomery, H.; Brown, W. *Phys. Rev.* **1956**, *103*, 865–870.

[7] Many, A.; Goldstein, Y.; Grover, N. *Semiconductor Surfaces*; North-Holland Publishing Co.: Amsterdam, 1965.

[8] Gerlich, D.; Cullen, G.; Amick, J. *J. Electrochem. Soc.* **1962**, *109*, 133–138.

[9] Gstrein, F.; Michalak, D.; Royea, W.; Lewis, N. *J. Phys. Chem. B* **2002**, *106*, 2950–2961.

[10] Gaubas, E.; Vanhellemont, J. *Appl. Phys. Lett.* **2006**, *89*, 142106.

[11] Yang, M.; Wu, R.; Q., C.; W.S., D.; Feng, Y.; Chai, J.; Pan, J.; Wang, S. *Appl. Phys. Lett.* **2009**, *94*, 142903.

[12] Hovis, J.; Hamers, R.; Greenlief, C. *Surf. Sci.* **1999**, *440*, L815–L819.

[13] Perego, M.; Scarel, G.; Fanciulli, M.; Fedushkin, I.; Skatova, A. A. *Appl. Phys. Lett.* **2007**, *90*, 162115.

[14] Tabet, N.; Faiz, M.; Hamdan, N.; Hussain, Z. *Surf. Sci.* **2003**, *523*, 68–72.

[15] Kingston, R. *Phys. Rev.* **1955**, *98*, 1766–1775.

[16] Tsipas, P.; Dimoulas, A. *Appl. Phys. Lett.* **2009**, *94*, 012114.

[17] Broqvist, P.; Alkauska, A.; Pasquarello, A. *Phys. Rev. B* **2008**, *78*, 075203.

[18] Hunger, R.; Fritsche, R.; Jaeckel, B.; Jaegermann, W.; Webb, L.; Lewis, N. *Phys. Rev. B* **2005**, *72*, 045317.

[19] Yu, H.; Webb, L.; Ries, R.; Solares, S.; Goddard, W.; Heath, J.; Lewis, N. *J. Phys. Chem. B* **2005**, *109*, 671–674.

[20] Rivillion, S.; Chabal, Y. *J. Phys. IV* **2006**, *132*, 195–198.

[21] Jaeckel, B.; Hunger, R.; Webb, L.; Jaegermann, W.; Lewis, N. *J. Phys. Chem. C* **2007**, *111*, 18204–18213.

[22] Lopinski, G.; Eves, B.; Hul'ko, O.; Mark, C.; Patitsas, N.; Boukherroub, R.; Ward, T. *Phys. Rev. B* **2005**, *71*, 125308.

[23] Cao, P.; Yu, H.; Heath, J. *J. Phys. Chem. B* **2006**, *110*, 2006.

[24] Webb, L.; Rivillon, S.; Michalak, D.; Chabal, Y.; Lewis, N. *J. Phys. Chem. B* **2006**, *110*, 7349–7356.

[25] Bruening, M.; Moons, E.; Yaron-Marcovich, D.; Cahen, D.; Libman, J.; Shanzer, A. *J. Am. Chem. Soc.* **1994**, *116*, 2972–2977.

[26] Maldonado, S.; Lewis, N. *J. Electrochem. Soc.* **2009**, *156*, H123–H128.